Strong vertices of bottom mesons B and B^* and bottomonia Υ, η_b*

Jie Lu (卢杰)[1,2] Guo-Liang Yu (于国梁)[1,2†] Zhi-Gang Wang (王志刚)[1‡] Bin Wu (吴彬)[1]

[1]Department of Mathematics and Physics, North China Electric Power University, Baoding 071003, China
[2]Hebei Key Laboratory of Physics and Energy Technology, North China Electric Power University, Baoding 071000, China

Abstract: In this study, the strong coupling constants of vertices $BB\Upsilon$, $BB^*\Upsilon$, $B^*B^*\Upsilon$, $BB^*\eta_b$, and $B^*B^*\eta_b$ are analyzed in the framework of QCD sum rules. All possible off-shell cases and the contributions of vacuum condensate terms including $\langle\bar{q}q\rangle$, $\langle\bar{q}g_s\sigma Gq\rangle$, $\langle g_s^2G^2\rangle$, $\langle f^3G^3\rangle$, and $\langle\bar{q}q\rangle\langle g_s^2G^2\rangle$ are considered. The momentum dependent strong coupling constants are first calculated and then fitted into the analytical function $g(Q^2)$, which is extrapolated to time-like regions to obtain the final values of strong coupling constants. The final results are $g_{BB\Upsilon}=40.67^{+7.55}_{-4.20}$, $g_{BB^*\Upsilon}=11.58^{+2.19}_{-1.09}$ GeV^{-1}, $g_{B^*B^*\Upsilon}=57.02^{+5.32}_{-5.31}$, $g_{BB^*\eta_b}=23.39^{+4.74}_{-2.30}$, and $g_{B^*B^*\eta_b}=12.49^{+2.12}_{-1.35}$ GeV^{-1}. These strong coupling constants are important input parameters that reflect the dynamic properties of the interactions among the mesons and quarkonia.

Keywords: bottom meson, strong coupling constants, QCD sum rules

DOI: 10.1088/1674-1137/ad061d

I. INTRODUCTION

The suppression of J/ψ production in relativistic heavy ion collisions is an important signature to identify the quark-gluon plasma [1]. Because of the color screening, the dissociation of J/ψ in the quark-gluon plasma would lead to a reduction of its production. The bottomonia are also sensitive to the color screening; therefore, the Υ suppression in heavy ion collisions can also be considered as a signature to identify the quark-gluon plasma [2, 3]. Some attempts to analyze the heavy quarkonium absorptions using the effective Lagrangians in meson exchange models have been successful [4−8]. Further, the absorption cross sections can be calculated based on the interactions among the mesons and quarkonia, where the strong coupling constants are taken as an important input parameter. Meanwhile, accurate determination of the strong coupling constants plays an important role in understanding the effects of heavy quarkonium absorptions in hadronic matter [9]. Besides, the coupling constants among heavy quarkonia and heavy mesons are valuable for us to understand the final-state interactions in heavy quarkonium decays [9, 10].

The QCD sum rules and the light-cone QCD sum rules are powerful nonperturbative approaches in analyzing the strong coupling constants among the hadrons. In recent years, the strong vertices $DD^*\pi$, D^*D_sK, DD_s^*K, $BB^*\pi$, B^*B_sK, BB_s^*K, $DD\rho$, DD_sK^*, BB_sK^*, $DD^*\rho$, $DD_s^*K^*$, $BB_s^*K^*$, $D^*D^*\rho$, $B^*B^*\rho$, $BB_{s_0}K$, $B^*B_{s_1}K$, $DD_s^*K_1$, $BB_s^*K_1$, $D_s^*D_s\phi$, $D_2^*D^*\pi$, $D_{s_2}^*D^*K$, $D_2^*D\rho$, $D_2^*D\omega$, $D_{s_2}^*D_s\phi$, DDJ/ψ, DD^*J/ψ, D^*D^*J/ψ, $DD^*\eta_c$, $D^*D^*\eta_c$, and $D_sD_s^*\eta_c$ have been analyzed with the three-point QCD sum rules (QCDSR) [11−29], and the coupling constants of vertices $DD^*\pi$, D^*D_sK, DD_s^*K,$BB^*\pi$, $DD\rho$, DD_sK^*, $D_sD_s\phi$, $BB\rho$, $DD^*\rho$, $D_sD^*K^*$, $D_sD_s^*\phi$, $BB^*\rho$, $D^*D^*\pi$, $D^*D_s^*K$, $B^*B^*\pi$, $D^*D^*\rho$, $DD_0\pi$, $BB_0\pi$, D_0D_sK, $DD_{s_0}K$, $BB_{s_0}K$, $D_1D^*\pi$, $B_1B^*\pi$, $D_{s_1}D^*K$, $B_{s_1}B^*K$, $B_0B_1\pi$, $B_1B_2\pi$, $B_2B^*\pi$, $B_1B^*\rho$, $BB_1\rho$, $B_2B^*\rho$, and $B_1B_2\rho$ have been studied with the light-cone QCD sum rules (LCSR) [30−45]. In the early QCDSR and LCSR calculations, only the leading order contributions are considered, and the higher-order QCD corrections and subleading order contributions are often omitted. In recent years, some strong coupling constants were analyzed with the method of LCSR considering the higher-order QCD corrections and next leading power contributions [45, 46] or with the method of QCDSR considering higher dimension condensate terms [25−29]. These studies indicate the importance of considering the higher-order contributions for achieving accurate final results.

Received 14 August 2023; Accepted 23 October 2023; Published online 24 October 2023

* Supported by the National Natural Science Foundation of China (12175068), and Natural Science Foundation of Hebei Province, China (A2018502124)

† E-mail: yuguoliang2011@163.com
‡ E-mail: zgwang@aliyun.com

In our previous studies, the strong vertices B_cB_cJ/ψ, $B_cB_c\Upsilon$, $B_cB_c^*J/\psi$, and $B_cB_c^*\Upsilon$ were examined using the three-point QCD sum rules, and the operator product expansion (OPE) was truncated at the dimension of 4 [47]. Recently, a systematic analysis of the strong vertices of charmed mesons D and D^* as well as charmonia J/ψ and η_c was performed [29], and the OPE was truncated at dimension 7. As a continuation of these studies, the strong vertices of the bottom mesons B and B^* and the bottomonia Υ and η_b are systematically analyzed in the present study.

This article is organized as follows. After the introduction in Sec. I, the strong vertices $BB\Upsilon$, BB^*J/ψ, $B^*B^*\Upsilon$, $BB^*\eta_b$, and $B^*B^*\eta_b$ are analyzed with the QCD-SR in Sec. II, in which all off-shell cases of the intermediate mesons are considered. In the QCD side, the perturbative contribution and vacuum condensate terms are considered including $\langle\bar{q}q\rangle$, $\langle\bar{q}g_s\sigma Gq\rangle$, $\langle g_s^2G^2\rangle$, $\langle f^3G^3\rangle$, and $\langle\bar{q}q\rangle\langle g_s^2G^2\rangle$. Section III presents the numerical results and discussions, while our conclusions are summarized in Sec. IV.

II. QCD SUM RULES

First, the following three-point correlation function is introduced:

$$\Pi(p,p') = \mathrm{i}^2\int \mathrm{d}^4x\mathrm{d}^4y\mathrm{e}^{\mathrm{i}p'x}\mathrm{e}^{\mathrm{i}(p-p')y} \times\langle 0|T\{J_{M_3}(x)J_{M_2}(y)J^+_{M_1}(0)\}|0\rangle, \tag{1}$$

where T is the time ordered product, J is the meson interpolating current, and the subscripts M_1, M_2, and M_3 denote the mesons in each vertex. Here, M_2 represents the intermediate meson, which is off-shell. The assignments of the mesons for each vertex are listed in Table 1.

The bottom meson and bottomonium interpolating currents are taken as follows:

$$\begin{aligned} J_B(x) &= \bar{u}(x)\mathrm{i}\gamma_5 b(x),\\ J_{B^*}(x) &= \bar{u}(x)\gamma_\mu b(x),\\ J_\Upsilon(x) &= \bar{b}(x)\gamma_\mu b(x),\\ J_{\eta_b}(x) &= \bar{b}(x)\mathrm{i}\gamma_5 b(x). \end{aligned} \tag{2}$$

The correlation function is calculated on two sides, called the phenomenological side and the QCD side. According to the quark hadron duality, calculations of these two sides are coordinated, and the QCD sum rules about the properties of hadrons can be obtained.

A. Phenomenological side

On the phenomenological side, a complete set of hadronic states with the same quantum numbers as the interpolating currents $J^+_{M_1}$, J_{M_2} , and J_{M_3} is inserted into the correlation function. Then, the correlation function can be written as follows using the dispersion relation [24]:

$$\begin{aligned}\Pi(p,p') =& \frac{\langle 0|J_{M_3}(0)|M_3(p')\rangle\langle 0|J_{M_2}(0)|M_2(q)\rangle}{(m^2_{M_1}-p^2)(m^2_{M_3}-p'^2)(m^2_{M_2}-q^2)}\\ &\times\langle M_1(p)|J^+_{M_1}(0)|0\rangle\langle M_2(q)M_3(p')|M_1(p)\rangle\\ &+\ldots \end{aligned} \tag{3}$$

where the ellipsis denotes the contributions of higher resonances and continuum states. The meson vacuum matrix elements in Eq. (3) are expressed as follows:

$$\begin{aligned} \langle 0|J_B(0)|B\rangle &= \frac{f_Bm_B^2}{m_b},\\ \langle 0|J_{B^*}(0)|B^*\rangle &= f_{B^*}m_{B^*}\zeta_\mu,\\ \langle 0|J_\Upsilon(0)|\Upsilon\rangle &= f_\Upsilon m_\Upsilon\xi_\mu,\\ \langle 0|J_{\eta_b}(0)|\eta_b\rangle &= \frac{f_{\eta_b}m^2_{\eta_b}}{2m_b}, \end{aligned} \tag{4}$$

where f_B, f_{B^*}, f_Υ , and f_{η_b} are the meson decay constants, and ξ_μ and ζ_μ are the polarization vectors of Υ and B^*, respectively. All meson vertex matrix elements in Eq. (3) can be obtained using the following effective Lagrangian:

$$\begin{aligned}\mathscr{L} =& \mathrm{i}g_{BB\Upsilon}\Upsilon_\alpha(\partial^\alpha B\bar{B}-B\partial^\alpha\bar{B})\\ &-g_{B^*B^*\eta_b}\varepsilon^{\alpha\beta\rho\tau}\partial_\alpha B^*_\beta\partial_\rho\bar{B}^*_\tau\eta_b\\ &-g_{B^*B\Upsilon}\varepsilon^{\alpha\beta\rho\tau}\partial_\alpha\Upsilon_\beta(\partial_\rho B^*_\tau\bar{B}+B\partial_\rho\bar{B}^*_\tau)\end{aligned}$$

Table 1. Assignments of mesons M_1, M_2, and M_3 for each vertex, where M_2 denotes the off-shell meson.

Vertices	M_1	M_2 (off-shell)	M_3
$BB\Upsilon$	B	Υ	B
	B	B	Υ
$BB^*\Upsilon$	B^*	Υ	B
	B^*	B	Υ
	B	B^*	Υ
$B^*B^*\Upsilon$	B^*	Υ	B^*
	B^*	B^*	Υ
$BB^*\eta_b$	B	η_b	B^*
	B^*	B	η_b
	B	B^*	η_b
$B^*B^*\eta_b$	B^*	η_b	B^*
	B^*	B^*	η_b

$$
\begin{aligned}
&+\mathrm{i}g_{B^*B^*\Upsilon}[\Upsilon^\alpha(\partial_\alpha B^{*\beta}\bar{B}^*_\beta - B^{*\beta}\partial_\alpha\bar{B}^*_\beta)\\
&+(\partial_\alpha\Upsilon_\beta B^{*\beta} - \Upsilon_\beta\partial_\alpha B^{*\beta})\bar{B}^{*\alpha}\\
&+B^{*\alpha}(\Upsilon^\beta\partial_\alpha\bar{B}^*_\beta - \partial_\alpha\Upsilon_\beta\bar{B}^{*\beta})]\\
&+\mathrm{i}g_{B^*B\eta_b}[B^{*\alpha}(\partial_\alpha\eta_b\bar{B} - \eta_b\partial_\alpha\bar{B})\\
&+(\partial_\alpha\eta_b B - \eta_b\partial_\alpha B)\bar{B}^{*\alpha}]. \qquad (5)
\end{aligned}
$$

According to this Lagrangian, all vertex matrix elements can be written as

$$
\begin{aligned}
&\langle B(p')\Upsilon(q)|B(p)\rangle = g^{\Upsilon}_{BB\Upsilon}(q^2)\xi^*_\alpha(p+p')^\alpha,\\
&\langle B(q)\Upsilon(p')|B(p)\rangle = g^{B}_{BB\Upsilon}(q^2)\xi_\alpha(p+q)^\alpha,\\
&\langle B(p')\Upsilon(q)|B^*(p)\rangle = -g^{\Upsilon}_{BB^*\Upsilon}(q^2)\varepsilon^{\alpha\beta\rho\tau}\xi_\alpha\zeta_\beta p_\rho p'_\tau,\\
&\langle B(q)\Upsilon(p')|B^*(p)\rangle = -g^{B}_{BB^*\Upsilon}(q^2)\varepsilon^{\alpha\beta\rho\tau}\xi_\alpha\zeta_\beta p_\rho p'_\tau,\\
&\langle B^*(q)\Upsilon(p')|B(p)\rangle = g^{B^*}_{BB^*\Upsilon}(q^2)\varepsilon^{\alpha\beta\rho\tau}\xi_\alpha\zeta_\beta p'_\rho p_\tau,\\
&\langle B^*(p')\Upsilon(q)|B^*(p)\rangle = g^{\Upsilon}_{B^*B^*J/\psi}[(p^\alpha+p'^\alpha)\xi^*_\alpha\zeta'^\beta\zeta^*_\beta\\
&-(p^\alpha+q^\alpha)\zeta'^*_\alpha\xi^*_\beta\zeta^\beta - (p'^\alpha-q^\alpha)\zeta_\alpha\xi^{*\beta}\zeta^*_\beta],\\
&\langle B^*(q)\Upsilon(p')|B^*(p)\rangle = g^{B^*}_{B^*B^*\Upsilon}[(p^\alpha+q^\alpha)\xi^*_\alpha\zeta'^\beta\varepsilon^*_\beta\\
&-(p^\alpha+p'^\alpha)\zeta'^*_\alpha\xi^*_\beta\zeta^\beta - (q^\alpha-p'^\alpha)\zeta_\alpha\xi^{*\beta}\zeta'^*_\beta],\\
&\langle B(p')\eta_b(q)|B^*(p)\rangle = -g^{\eta_b}_{BB^*\eta_b}(q^2)\zeta_\alpha(q-p')^\alpha,\\
&\langle B(q)\eta_b(p')|B^*(p)\rangle = -g^{B}_{BB^*\eta_b}(q^2)\zeta_\alpha(p'-q)^\alpha,\\
&\langle B^*(q)\eta_b(p')|B(p)\rangle = -g^{B^*}_{BB^*\eta_b}(q^2)\zeta^*_\alpha(p+p')^\alpha,\\
&\langle B^*(p')\eta_b(q)|B^*(p)\rangle = -g^{\eta_b}_{B^*B^*\eta_b}(q^2)\varepsilon^{\alpha\beta\rho\tau}\zeta_\alpha\zeta'^*_\beta p_\rho p'_\tau,\\
&\langle B^*(q)\eta_b(p')|B^*(p)\rangle = -g^{D^*}_{B^*B^*\eta_b}(q^2)\varepsilon^{\alpha\beta\rho\tau}\zeta'_\alpha\zeta^*_\beta p_\rho q_\tau, \qquad (6)
\end{aligned}
$$

where ξ_α and $\zeta^{(')}_\alpha$ are the polarization vectors of Υ and B^*, respectively; $q = p - p'$; and $\varepsilon^{\alpha\beta\rho\tau}$ is the 4-dimension Levi-Civita tensor. The subscript of g in Eq. (6) denotes the type of strong vertex, and the superscript denotes the intermediate meson, which is off-shell. From Eqs. (3)−(6), the expressions of the correlation function on the phenomenological side can be obtained and divided into different tensor structures. In general, different tensor structures for a correlation function lead to the same result; thus, choosing an appropriate structure to analyze the strong vertex is acceptable.

B. The QCD side

On the QCD side, we contract the quark fields with Wick's theorem, followed by the operator product expansion (OPE). After the first process, the correlation functions for vertices $BB\Upsilon$, $BB^*\Upsilon$, $B^*B^*\Upsilon$, $BB^*\eta_b$, and $B^*B^*\eta_b$ can be written as

$$
\begin{aligned}
\Pi^{\Upsilon}_{\mu}(p,p') &= \int \mathrm{d}^4x\mathrm{d}^4y\mathrm{e}^{\mathrm{i}p'x}\mathrm{e}^{\mathrm{i}(p-p')y}\\
&\times\mathrm{Tr}\{B^{nk}(y)\gamma_5 U^{km}(-x)\gamma_5 B^{mn}(x-y)\gamma_\mu\},\\
\Pi^{B}_{\mu}(p,p') &= \int \mathrm{d}^4x\mathrm{d}^4y\mathrm{e}^{\mathrm{i}p'x}\mathrm{e}^{\mathrm{i}(p-p')y}\\
&\times\mathrm{Tr}\{\gamma_\mu B^{nk}(x)\gamma_5 U^{km}(-y)\gamma_5 B^{mn}(y-x)\}, \qquad (7)\\
\Pi^{\Upsilon}_{\mu\nu}(p,p') &= -\mathrm{i}\int \mathrm{d}^4x\mathrm{d}^4y\mathrm{e}^{\mathrm{i}p'x}\mathrm{e}^{\mathrm{i}(p-p')y}\\
&\times\mathrm{Tr}\{B^{nk}(y)\gamma_\nu U^{km}(-x)\gamma_5 B^{mn}(x-y)\gamma_\mu\},\\
\Pi^{B}_{\mu\nu}(p,p') &= -\mathrm{i}\int \mathrm{d}^4x\mathrm{d}^4y\mathrm{e}^{\mathrm{i}p'x}\mathrm{e}^{\mathrm{i}(p-p')y}\\
&\times\mathrm{Tr}\{\gamma_\mu B^{nk}(x)\gamma_\nu U^{km}(-y)\gamma_5 B^{mn}(y-x)\},\\
\Pi^{B^*}_{\mu\nu}(p,p') &= -\mathrm{i}\int \mathrm{d}^4x\mathrm{d}^4y\mathrm{e}^{\mathrm{i}p'x}\mathrm{e}^{\mathrm{i}(p-p')y}\\
&\times\mathrm{Tr}\{\gamma_\mu B^{nk}(x)\gamma_5 U^{km}(-y)\gamma_\nu B^{mn}(y-x)\}, \qquad (8)\\
\Pi^{\Upsilon}_{\mu\nu\sigma}(p,p') &= \int \mathrm{d}^4x\mathrm{d}^4y\mathrm{e}^{\mathrm{i}p'x}\mathrm{e}^{\mathrm{i}(p-p')y}\\
&\times\mathrm{Tr}\{B^{nk}(y)\gamma_\nu U^{km}(-x)\gamma_\sigma B^{mn}(x-y)\gamma_\mu\},\\
\Pi^{B^*}_{\mu\nu\sigma}(p,p') &= \int \mathrm{d}^4x\mathrm{d}^4y\mathrm{e}^{\mathrm{i}p'x}\mathrm{e}^{\mathrm{i}(p-p')y}\\
&\times\mathrm{Tr}\{\gamma_\mu B^{nk}(x)\gamma_\sigma U^{km}(-y)\gamma_\nu B^{mn}(y-x)\}, \qquad (9)\\
\Pi^{\eta_b}_{\mu}(p,p') &= \int \mathrm{d}^4x\mathrm{d}^4y\mathrm{e}^{\mathrm{i}p'x}\mathrm{e}^{\mathrm{i}(p-p')y}\\
&\times\mathrm{Tr}\{B^{nk}(y)\gamma_\mu U^{km}(-x)\gamma_5 B^{mn}(x-y)\gamma_5\},\\
\Pi^{B}_{\mu}(p,p') &= \int \mathrm{d}^4x\mathrm{d}^4y\mathrm{e}^{\mathrm{i}p'x}\mathrm{e}^{\mathrm{i}(p-p')y}\\
&\times\mathrm{Tr}\{\gamma_5 B^{nk}(x)\gamma_\mu U^{km}(-y)\gamma_5 B^{mn}(y-x)\},\\
\Pi^{B^*}_{\mu}(p,p') &= \int \mathrm{d}^4x\mathrm{d}^4y\mathrm{e}^{\mathrm{i}p'x}\mathrm{e}^{\mathrm{i}(p-p')y}\\
&\times\mathrm{Tr}\{\gamma_5 B^{nk}(x)\gamma_5 U^{km}(-y)\gamma_\mu B^{mn}(y-x)\}, \qquad (10)\\
\Pi^{\eta_b}_{\mu\nu}(p,p') &= -\mathrm{i}\int \mathrm{d}^4x\mathrm{d}^4y\mathrm{e}^{\mathrm{i}p'x}\mathrm{e}^{\mathrm{i}(p-p')y}\\
&\times\mathrm{Tr}\{B^{nk}(y)\gamma_\nu U^{km}(-x)\gamma_\mu B^{mn}(x-y)\gamma_5\},\\
\Pi^{B^*}_{\mu\nu}(p,p') &= -\mathrm{i}\int \mathrm{d}^4x\mathrm{d}^4y\mathrm{e}^{\mathrm{i}p'x}\mathrm{e}^{\mathrm{i}(p-p')y}\\
&\times\mathrm{Tr}\{\gamma_5 B^{nk}(x)\gamma_\mu U^{km}(-y)\gamma_\nu B^{mn}(y-x)\}. \qquad (11)
\end{aligned}
$$

The superscripts of Π in the above equations denote the intermediate mesons. $U^{ij}(x)$ and $B^{ij}(x)$ are the full propagators of $u(d)$ and b quarks, respectively, which have the following forms [48]:

$$
\begin{aligned}
U^{ij}(x) =& \frac{\mathrm{i}\delta^{ij}\not{x}}{2\pi^2x^4} - \frac{\delta^{ij}m_q}{4\pi^2x^4} - \frac{\delta^{ij}\langle\bar{q}q\rangle}{12} + \frac{\mathrm{i}\delta^{ij}\not{x}m_q\langle\bar{q}q\rangle}{48} \\
& - \frac{\delta^{ij}x^2\langle\bar{q}g_s\sigma Gq\rangle}{192} + \frac{\mathrm{i}\delta^{ij}x^2\not{x}m_q\langle\bar{q}g_s\sigma Gq\rangle}{1152} \\
& - \frac{\mathrm{i}g_sG^a_{\alpha\beta}t^a_{ij}(\not{x}\sigma^{\alpha\beta}+\sigma^{\alpha\beta}\not{x})}{32\pi^2x^2} - \frac{\mathrm{i}\delta^{ij}x^2\not{x}g_s^2\langle\bar{q}q\rangle^2}{7776} \\
& - \frac{\delta^{ij}x^4\langle\bar{q}q\rangle\langle g_s^2GG\rangle}{27648} - \frac{\langle\bar{q}^j\sigma^{\mu\nu}q^i\rangle\sigma_{\mu\nu}}{8} \\
& - \frac{\langle\bar{q}^j\gamma^\mu q^i\rangle\gamma_\mu}{4} + \ldots, \\
B^{ij}(x) =& \frac{\mathrm{i}}{(2\pi)^4}\int \mathrm{d}^4k\mathrm{e}^{-\mathrm{i}k\cdot x}\Big\{\frac{\delta^{ij}}{\not{k}-m_b} \\
& - \frac{g_sG^n_{\alpha\beta}t^n_{ij}}{4}\frac{\sigma^{\alpha\beta}(\not{k}+m_b)+(\not{k}+m_b)\sigma^{\alpha\beta}}{(k^2-m_b^2)^2} \\
& + \frac{g_sD_\alpha G^n_{\beta\lambda}t^n_{ij}(f^{\lambda\beta\alpha}+f^{\lambda\alpha\beta})}{3(k^2-m_b^2)^4} \\
& - \frac{g_s^2(t^at^b)_{ij}G^a_{\alpha\beta}G^b_{\mu\nu}(f^{\alpha\beta\mu\nu}+f^{\alpha\mu\beta\nu}+f^{\alpha\mu\nu\beta})}{4(k^2-m_b^2)^5} \\
& + \ldots\Big\},
\end{aligned} \tag{12}
$$

where $\langle g_s^2G^2\rangle = \langle g_s^2G^n_{\alpha\beta}G^{n\alpha\beta}\rangle$, $D_\alpha = \partial_\alpha - \mathrm{i}g_sG^n_\alpha t^n$, and $t^n = \frac{\lambda^n}{2}$. $\lambda^n(n=1,\ldots,8)$ are the Gell-Mann matrices; i and j are color indices; $q = u(d)$; $\sigma_{\alpha\beta} = \frac{\mathrm{i}}{2}[\gamma_\alpha,\gamma_\beta]$; and $f^{\lambda\alpha\beta}$ and $f^{\alpha\beta\mu\nu}$ have the following forms:

$$
f^{\lambda\alpha\beta} = (\not{k}+m_b)\gamma^\lambda(\not{k}+m_b)\gamma^\alpha(\not{k}+m_b)\gamma^\beta(\not{k}+m_b), \tag{13}
$$

$$
\begin{aligned}
f^{\alpha\beta\mu\nu} =& (\not{k}+m_b)\gamma^\alpha(\not{k}+m_b)\gamma^\beta(\not{k}+m_b) \\
& \gamma^\mu(\not{k}+m_b)\gamma^\nu(\not{k}+m_b).
\end{aligned} \tag{14}
$$

As stated in Sec. II.A, the different correlation functions, i.e., Π_μ, $\Pi_{\mu\nu}$, and $\Pi_{\mu\nu\sigma}$, in Eqs. (7)−(11) can be expanded into different tensor structures:

$$
\begin{aligned}
\Pi_\mu(p,p') =& \Pi_1(p^2,p'^2,q^2)p_\mu + \Pi_2(p^2,p'^2,q^2)p'_\mu, \\
\Pi_{\mu\nu}(p,p') =& \Pi(p^2,p'^2,q^2)\varepsilon_{\mu\nu\alpha\beta}p^\alpha p'^\beta, \\
\Pi_{\mu\nu\sigma}(p,p') =& \Pi_1(p^2,p'^2,q^2)p_\mu g_{\nu\sigma} \\
& + \Pi_2(p^2,p'^2,q^2)p_\mu p_\nu p_\sigma + \Pi_3(p^2,p'^2,q^2)p'_\mu p_\nu p_\sigma \\
& + \Pi_4(p^2,p'^2,q^2)p_\sigma g_{\mu\nu} + \Pi_5(p^2,p'^2,q^2)p_\mu p'_\nu p_\sigma \\
& + \Pi_6(p^2,p'^2,q^2)p'_\mu g_{\nu\sigma} + \Pi_7(p^2,p'^2,q^2)p_\mu p_\nu p'_\sigma \\
& + \Pi_8(p^2,p'^2,q^2)p'_\nu g_{\mu\sigma} + \Pi_9(p^2,p'^2,q^2)p'_\mu p'_\nu p_\sigma \\
& + \Pi_{10}(p^2,p'^2,q^2)p'_\sigma g_{\mu\nu} + \Pi_{11}(p^2,p'^2,q^2)p'_\mu p_\nu p'_\sigma \\
& + \Pi_{12}(p^2,p'^2,q^2)p_\mu p'_\nu p'_\sigma + \Pi_{13}(p^2,p'^2,q^2)p_\nu g_{\mu\sigma} \\
& + \Pi_{14}(p^2,p'^2,q^2)p'_\mu p'_\nu p'_\sigma,
\end{aligned} \tag{15}
$$

where $g_{\mu\nu}$ is the metric tensor. On the right side of the above equations, Π without the Lorentz index is commonly called the scalar invariant amplitude. To obtain the strong coupling constant, an appropriate scalar amplitude should be selected to carry out the analysis [14]. Considering vertex $B^*B^*\Upsilon$ as an example, its correlation function $\Pi_{\mu\nu\sigma}$ has fourteen tensor structures. In principle, it is reasonable to perform the calculations with each structure; in this paper, we choose the structure $p_\mu g_{\nu\sigma}$ to analyze the strong vertex $B^*B^*\Upsilon$.

The scalar invariant amplitudes on the QCD side are represented as Π^{OPE}, which can be divided into two parts:

$$
\Pi^{\mathrm{OPE}} = \Pi^{\mathrm{pert}} + \Pi^{\mathrm{non-pert}}, \tag{16}
$$

where Π^{pert} refers to the perturbative part, and $\Pi^{\mathrm{non-pert}}$ denotes the non-perturbative contributions including $\langle\bar{q}q\rangle$, $\langle g_s^2G^2\rangle$, $\langle\bar{q}g_s\sigma Gq\rangle$, $\langle f^3G^3\rangle$, and $\langle\bar{q}q\rangle\langle g_s^2G^2\rangle$. The perturbative part and the $\langle g_s^2G^2\rangle$ and $\langle f^3G^3\rangle$ terms can be written as follows according to the dispersion relation:

$$
\Pi(p,p') = -\int_0^\infty\int_0^\infty \frac{\rho(s,u,q^2)}{(s-p^2)(u-p'^2)}\mathrm{d}s\mathrm{d}u,
$$

where

$$
\begin{aligned}
\rho(s,u,q^2) =& \rho^{\mathrm{pert}}(s,u,q^2) + \rho^{\langle g_s^2G^2\rangle}(s,u,q^2) \\
& + \rho^{\langle f^3G^3\rangle}(s,u,q^2)
\end{aligned} \tag{17}
$$

and $s = p^2$, $u = p'^2$, and $q = p - p'$. The QCD spectral density $\rho(s,u,q^2)$ can be obtained by Cutkosky's rules [49] (see Fig. 1), the calculation for which is detailed in Ref. [29]. Moreover, we consider the contributions of $\langle\bar{q}q\rangle$, $\langle\bar{q}g_s\sigma Gq\rangle$, and $\langle\bar{q}q\rangle\langle g_s^2G^2\rangle$. The Feynman diagrams for all of these condensate terms can be classified into two groups, as illustrated in Figs. 2 and 3.

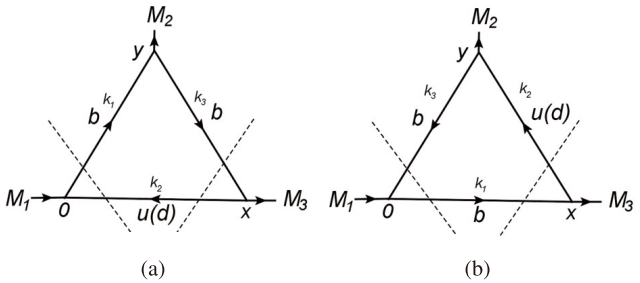

Fig. 1. Perturbative contributions for $\Upsilon(\eta_b)$ (a) and $B(B^*)$ (b) off-shell. The dashed lines denote the Cutkosky cuts.

We take the change in variables $p^2 \to -P^2$, $p'^2 \to -P'^2$, and $q^2 \to -Q^2$ and perform double Borel transformation on both the phenomenological and QCD sides. The variables P^2 and P'^2 are replaced by T_1^2 and T_2^2, respectively, where T_1 and T_2 are called the Borel parameters. In this article, we take $T^2 = T_1^2$ and $T_2^2 = kT_1^2 = kT^2$, where k is a constant related to meson mass, with different values for different vertices, as presented in Table 2. Finally, the sum rules for the coupling constants can be obtained by matching the phenomenological and QCD sides according to the quark-hadron duality. The momentum dependent strong coupling constant can be written as

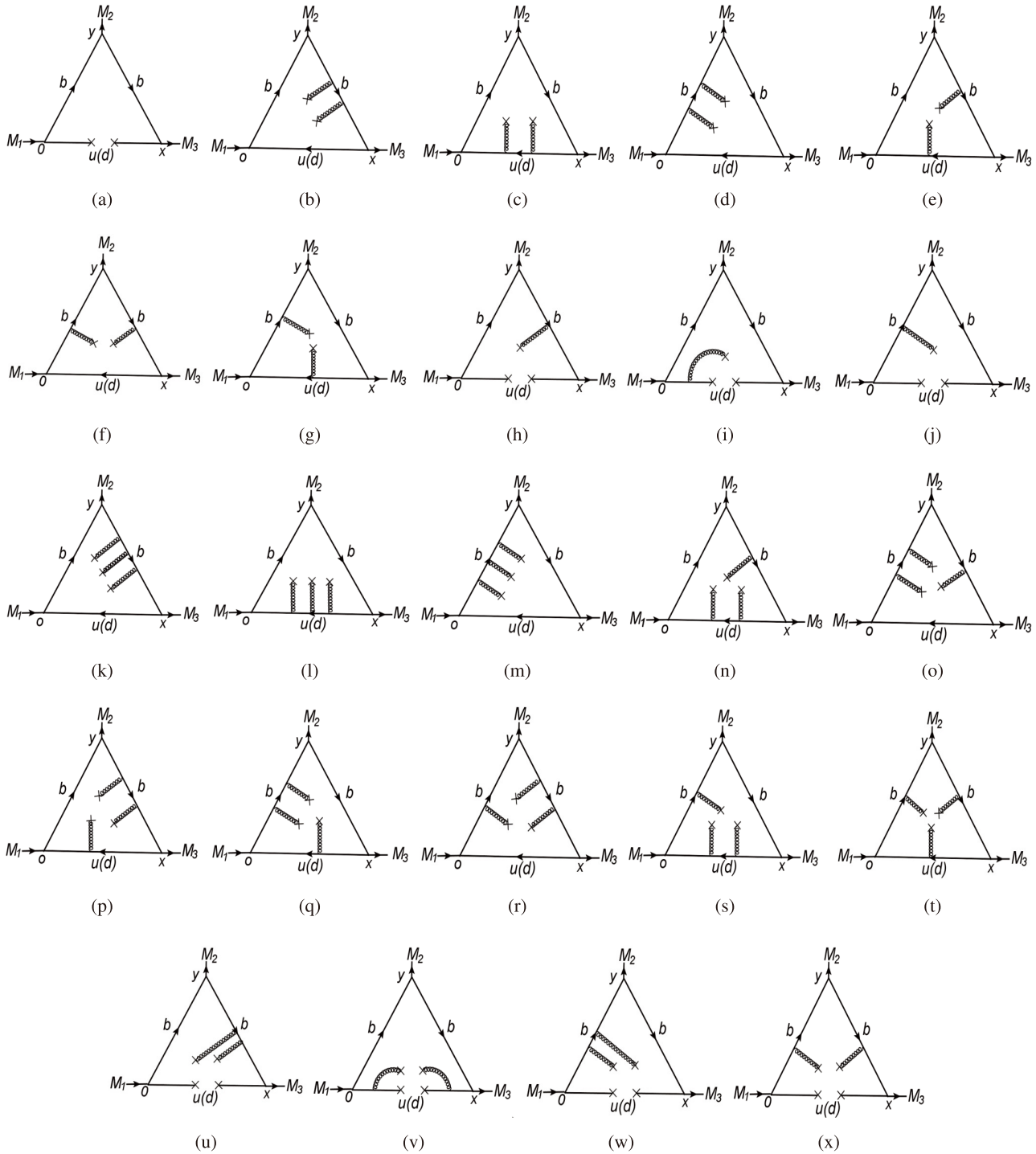

Fig. 2. Contributions of the non-perturbative parts for $\Upsilon(\eta_b)$ off-shell.

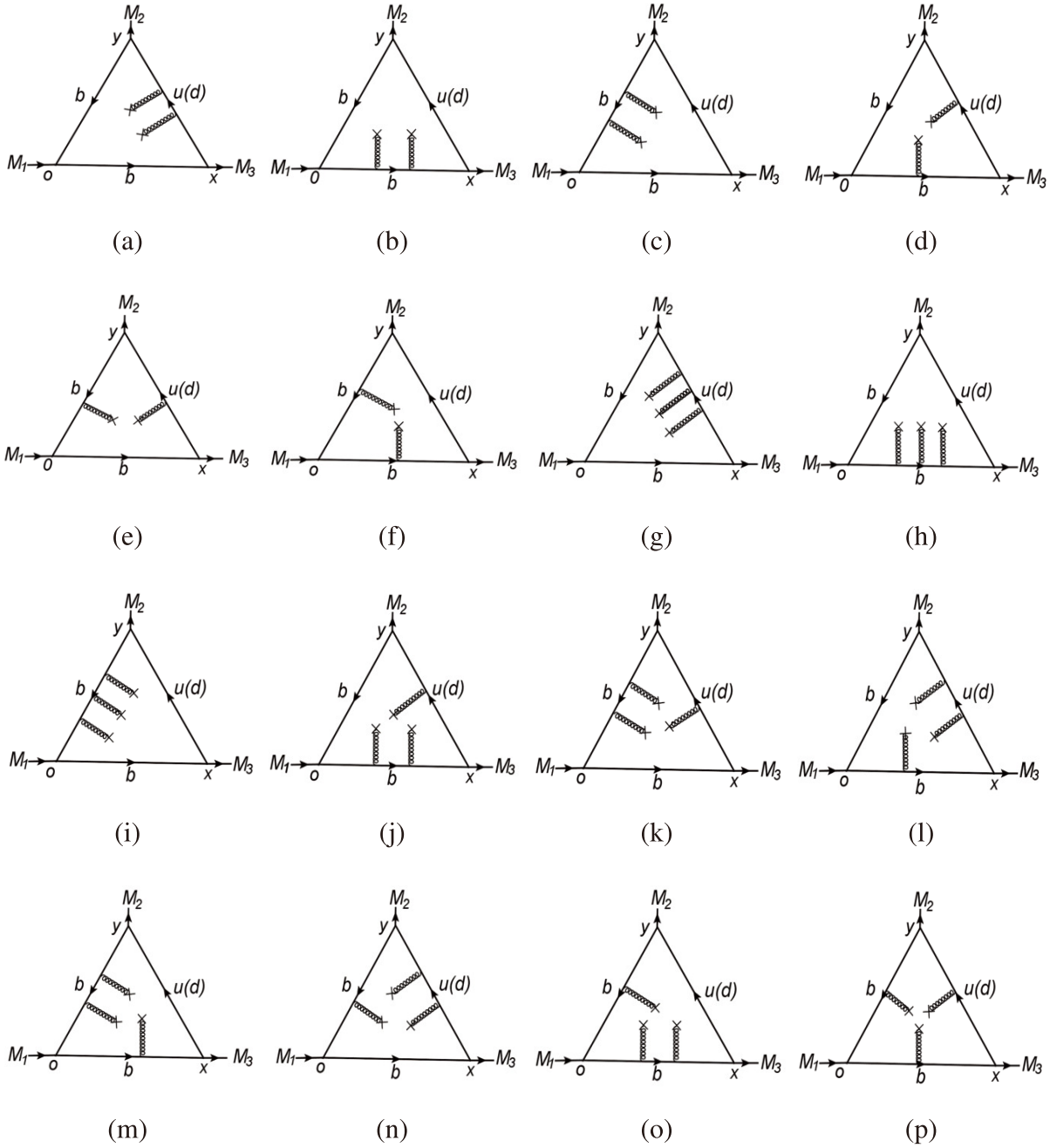

Fig. 3. Contributions of the non-perturbative parts for $B(B^*)$ off-shell.

$$g(Q^2)=\frac{-\int_{s_1}^{s_0}\int_{u_1}^{u_0}\rho(s,u,Q^2)\mathrm{e}^{-s/T^2}\mathrm{e}^{-u/kT^2}\mathrm{d}s\mathrm{d}u+\mathscr{B}\mathscr{B}[\Pi^{\mathrm{non-pert}}]}{\frac{E}{(m_{M_2}^2+Q^2)}\mathrm{e}^{-m_{M_1}^2/T^2}\mathrm{e}^{-m_{M_3}^2/kT^2}} \tag{18}$$

where $\mathscr{B}\mathscr{B}$ stands for the double Borel transformation, and E is a factor related to meson masses and decay constants (see Table 2). From this equation, we can also see that the threshold parameters s_0 and u_0 in the dispersion integral are introduced. These parameters are used to eliminate the contributions of higher resonances and continuum states in Eq. (3). They commonly fulfill the relations $m_{\mathrm{i}}^2 < s_0 < m_{\mathrm{i}}'^2$ and $m_{\mathrm{o}}^2 < u_0 < m_{\mathrm{o}}'^2$, where subscripts i and o represent incoming and outcoming mesons, respectively. m and m' are the masses of the ground and first excited states of the mesons. Generally, $m' = m + \Delta$, where Δ is taken as a value in the range of 0.4 ~ 0.6 GeV [24].

The strong coupling constant in Eq. (18) is momentum dependent, similar to the run coupling constant α_s. To obtain the final results of the strong coupling con-

Table 2. Parameters k and E for different vertices and off-shell cases.

Vertices	off-shell	k	E
$BB\Upsilon$	Υ	1	$\frac{f_B^2 m_B^4 f_\Upsilon m_\Upsilon}{m_b^2}$
	B	$\frac{m_\Upsilon^2}{m_{B^*}^2}$	$\frac{2 f_B^2 m_B^4 f_\Upsilon m_\Upsilon}{m_b^2}$
$BB^*\Upsilon$	Υ	$\frac{m_{B^*}^2}{m_B^2}$	
	B	$\frac{m_\Upsilon^2}{m_{B^*}^2}$	$-\frac{f_B m_B^2 f_{B^*} m_{B^*} f_\Upsilon m_\Upsilon}{m_b}$
	B^*	$\frac{m_\Upsilon^2}{m_B^2}$	
$B^*B^*\Upsilon$	Υ	1	$-f_{B^*}^2 m_{B^*}^2 f_\Upsilon m_\Upsilon$
	B^*	$\frac{m_\Upsilon^2}{m_B^2}$	$-2 f_{B^*}^2 m_{B^*}^2 f_\Upsilon m_\Upsilon$
$BB^*\eta_b$	η_b	$\frac{m_{B^*}^2}{m_B^2}$	$-\frac{f_B m_B^2 f_{B^*} m_{B^*} f_{\eta_b} m_{\eta_b}^2}{m_b^2}$
	B	$\frac{m_{\eta_b}^2}{m_{B^*}^2}$	
	B^*	$\frac{m_{\eta_b}^2}{m_B^2}$	$\frac{f_B m_B^2 f_{B^*} m_{B^*} f_{\eta_b} m_{\eta_b}^2 (m_{\eta_b}^2 + m_{B^*}^2 - m_B^2)}{2 m_b^2 m_{B^*}^2}$
$B^*B^*\eta_b$	η_b	1	$-\frac{f_{B^*}^2 m_{B^*}^2 f_{\eta_b} m_{\eta_b}^2}{2 m_b^2}$
	B^*	$\frac{m_{\eta_b}^2}{m_{B^*}^2}$	

stant, it is necessary to extrapolate the results obtained from Eq. (18) into time-like regions ($Q^2 < 0$). This process is realized by fitting $g(Q^2)$ into appropriate analytical functions and setting ($Q^2 = -m_{\rm on-shell}^2$).

III. NUMERICAL RESULTS AND DISCUSSIONS

All input parameters are taken as the standard values such as the hadronic masses and decay constants $m_B = 5.28$ GeV [50], $m_{B^*} = 5.33$ GeV [50], $m_\Upsilon = 9.46$ GeV [50], $m_{\eta_b} = 9.399$ GeV [50], $f_B = 0.192 \pm 0.013$ GeV [51], $f_{B^*} = 0.213 \pm 0.018$ GeV [51], $f_\Upsilon = 0.7$ GeV [50], and $f_{\eta_b} = 0.667 \pm 0.007$ GeV [52]. The vacuum condensates are also adopted as the standard values, which are $\langle\bar{q}q\rangle = -(0.23 \pm 0.01)^3$ GeV^3[50], $\langle\bar{q}g_s\sigma Gq\rangle = m_0^2\langle\bar{q}q\rangle$[50], $m_0^2 = 0.8 \pm 0.1$ GeV^2 [53−55], $\langle g_s^2 G^2\rangle = 0.88 \pm 0.15$ GeV^4 [53−55], and $\langle f^3 G^3\rangle = (8.8 \pm 5.5)$ GeV$^2\langle g_s^2 G^2\rangle$ [53−55]. The $\overline{\rm MS}$ mass of light and heavy quarks is adopted from the Particle Data Group [50], where $m_{u(d)}(\mu = 1{\rm GeV}) = 0.006 \pm 0.001$ GeV and $m_b(m_b) = 4.18 \pm 0.03$ GeV. In principle, both the vacuum condensates and the $\overline{\rm MS}$masses of light and heavy quarks are energy-scale dependent. For the B meson, the influences of vacuum condensates and the masses of light quarks are smaller than that of the bottom quark. More specifically, the mass of the bottom quark has a significant influence on the results, and its energy-scale dependency should be considered and discussed. The energy-scale dependent $\overline{\rm MS}$ mass of bottom quark can be expressed as follows according to the re-normalization group equation,

$$\begin{aligned} m_b(\mu) =& m_b(m_b)\left[\frac{\alpha_s(\mu)}{\alpha_s(m_b)}\right]^{\frac{12}{33-2n_f}} \\ \alpha_s(\mu) =& \frac{1}{b_0 t}\left[1 - \frac{b_1}{b_0^2}\frac{\log t}{t} \right. \\ & \left. + \frac{b_1^2(\log^2 t - \log t - 1) + b_0 b_2}{b_0^4 t^2}\right], \end{aligned} \tag{19}$$

where $t = \log\frac{\mu^2}{\Lambda_{\rm QCD}^2}$; $b_0 = \frac{33-2n_f}{12\pi}$; $b_1 = \frac{153-19n_f}{24\pi^2}$; $b_2 = (2857 - \frac{5033}{9}n_f + \frac{325}{27}n_f^2)/(128\pi^3)$; and $\Lambda_{\rm QCD} = 210$ MeV, 292 MeV, and 332 MeV for the flavors $n_f = 5, 4$, and 3, respectively [50]. In the framework of QCDSR, the final results should be obtained by selecting an appropriate energy-scale. In some similar research, the masses of heavy quarks in the energy-scale $\mu = m_Q$ were employed to obtain the coupling constants [24, 28]. In the present study, the mass of bottom quark in the energy-scale $\mu = m_b$ is also used to obtain the strong coupling constants [50]. The dependence of the strong coupling constants on energy-scales will be discussed at the end of this section.

According to Eq. (18), the strong coupling constant is a function of some input parameters such as the Borel parameter T^2, continuum thresholds s_0 and u_0, and square momentum Q^2. The Borel parameter T^2 is determined by two conditions, which are the pole dominance and convergence of OPE. To analyze the pole contribution, we first write

$$\begin{aligned} \Pi_{\rm pole}^{\rm OPE}(T^2) =& -\int_{s_1}^{s_0}\int_{u_1}^{u_0}\rho^{\rm OPE}(s,u,Q^2){\rm e}^{-\frac{s}{T^2}}{\rm e}^{-\frac{u}{kT^2}}{\rm d}s{\rm d}u \\ \Pi_{\rm cont}^{\rm OPE}(T^2) =& -\int_{s_0}^{\infty}\int_{u_0}^{\infty}\rho^{\rm OPE}(s,u,Q^2){\rm e}^{-\frac{s}{T^2}}{\rm e}^{-\frac{u}{kT^2}}{\rm d}s{\rm d}u. \end{aligned} \tag{20}$$

Meanwhile, the pole and continuum contributions are defined as [24]

$$\begin{aligned} {\rm Pole} =& \frac{\Pi_{\rm pole}^{\rm OPE}(T^2)}{\Pi_{\rm pole}^{\rm OPE}(T^2) + \Pi_{\rm cont}^{\rm OPE}(T^2)} \\ {\rm Continuum} =& \frac{\Pi_{\rm cont}^{\rm OPE}(T^2)}{\Pi_{\rm pole}^{\rm OPE}(T^2) + \Pi_{\rm cont}^{\rm OPE}(T^2)}. \end{aligned} \tag{21}$$

In addition, the continuum threshold parameters s_0 and u_0 are employed to include the pole contribution and suppress the contribution of higher resonances and con-

tinuum states. Their values commonly satisfy the relations $s_0 = (m_i + \Delta_i)^2$ and $u_0 = (m_o + \Delta_o)^2$, where the subscripts i and o represent the incoming and outcoming mesons, respectively. The values of Δ_i and Δ_o should be smaller than the experimental value of the distance between the ground and first excited states. In general, Δ_i and Δ_o are considered as 0.5 GeV.

Taking the strong coupling constant $g^{\Upsilon}_{BB'\Upsilon}$ as an example, we introduce the method of selection for the above parameters. Fixing $Q^2 = 3$ GeV^2 in Eq. (18), we first plot the strong coupling constant $g^{\Upsilon}_{BB'\Upsilon}$ for the Borel parameter T^2 at different values of s_0 and u_0; this dependence is shown in Fig. 4, indicating that the results have good stability when s_0 and u_0 are 31.14 ~ 35.76 GeV^2 (the corresponding values of Δ_i and Δ_o are 0.3 ~ 0.7 GeV). The pole and continuum contributions with variation of the Borel parameter T^2 are depicted in Fig. 5. In can be seen from this figure that the condition of pole dominance (≥40%) is satisfied in the range 17 GeV$^2 \leq T^2 \leq$ 19 GeV^2. The contributions of the total, perturbative, and all vacuum condensate terms for vertex $BB'\Upsilon$ are explicitly shown in Figs. 6 (a) and (b). These

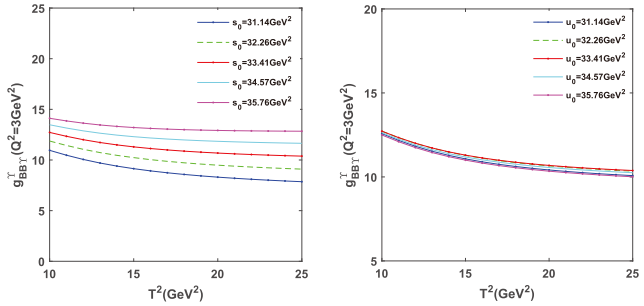

(a) (b)

Fig. 4. (color online) Strong coupling constants $g^{\Upsilon}_{BB'\Upsilon}$ for the Borel parameter T^2 at different values of s_0(a) and u_0(b).

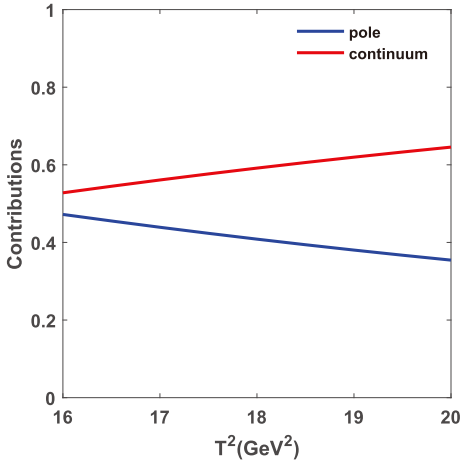

Fig. 5. (color online) Pole and continuum contributions with variation of the Borel parameter T^2 for the vertex $BB'\Upsilon$ in the Y off-shell case.

results demonstrate good stability with variation of Borel parameter T^2 in the range 17 GeV$^2 \leq T^2 \leq$ 19 GeV^2, indicating that the condition of OPE convergence is also satisfied. This flat region (17 GeV$^2 \leq T^2 \leq$ 19 GeV^2) is usually called the "Borel Window" and is used to extract the final results. According to a similar analysis with $g^{\Upsilon}_{BB'\Upsilon}$, the Borel Window for other strong vertices are also determined with $\Delta_i = \Delta_o = 0.5$ GeV, as shown in Fig. 6.

Considering different values of Q^2, the momentum dependent strong coupling constant $g(Q^2)$ can be obtained with the values of Q^2 being taken as 3 ~ 28 GeV^2 uniformly. The on-shell values of these coupling constants can be obtained by extrapolating the results ($g(Q^2)$) to the time-like regions ($Q^2 < 0$). This process is implemented by fitting $g(Q^2)$ with appropriate functions and setting the intermediate meson on-shell ($Q^2 = -m^2_{\text{on-shell}}$). To choose appropriate fitting functions, two conditions should be satisfied: first, the strong coupling constants should be well fitted in the space-like regions ($Q^2 > 0$); second, the values of the strong coupling constants in deep time-like regions should converge. In addition, the on-shell values for the same vertex in different off-shell cases should be as close to each other as possible. Considering the above requirements, the uncertainties of the fitting function selection can be greatly reduced. Taking the strong coupling constant $g_{BB'\Upsilon}$ as an example, $g(Q^2)$ can be fitted into two functions with Υ and B being off-shell cases, expressed as

$$\begin{aligned} C1: \quad & g^{\Upsilon}_{BB'\Upsilon}(Q^2) = 11.43\text{e}^{-0.013Q^2} \\ & g^{B}_{BB'\Upsilon}(Q^2) = 7.99\text{e}^{-0.062Q^2} - 1.20 \\ C2: \quad & g^{\Upsilon}_{BB'\Upsilon}(Q^2) = 11.78\text{e}^{0.02Q^2} - 0.45Q^2 \\ & g^{B}_{BB'\Upsilon}(Q^2) = 6.84\text{e}^{-0.072Q^2} - 0.03Q^2. \end{aligned} \tag{22}$$

Their fitting curves are shown in Fig. 7, where we can see that both the fitting curves $C1$ and $C2$ are well fitted in the space-like regions for Υ and B off-shell cases, and the on-shell values are well convergent. For the case of $g^{\Upsilon}_{BB'\Upsilon}$, the curve $C1$ (the blue solid line) is better fitted in the space-like regions than curve $C2$ (the blue dashed line). Thus, fitting function $C1$ is selected for $g_{BB'\Upsilon}$ in the Y off-shell case. For the B off-shell case, the curves $C1$ and $C2$ almost overlap each other in the space-like regions (the black solid and dashed lines). As stated above, the on-shell values for same vertex in different off-shell cases should be close to each other. We can see that curve $C1$ is more appropriate for this condition. Thus, $C1$ is selected to fit $g_{BB'\Upsilon}$ in the B off-shell case.

We know that the mass of the bottom quark is strongly energy-scale dependent, which also influences the final results obtained by QCDSR. Taking the coupling constant $g^{\Upsilon}_{BB'\Upsilon}(Q^2)$ as an example, we plot this de-

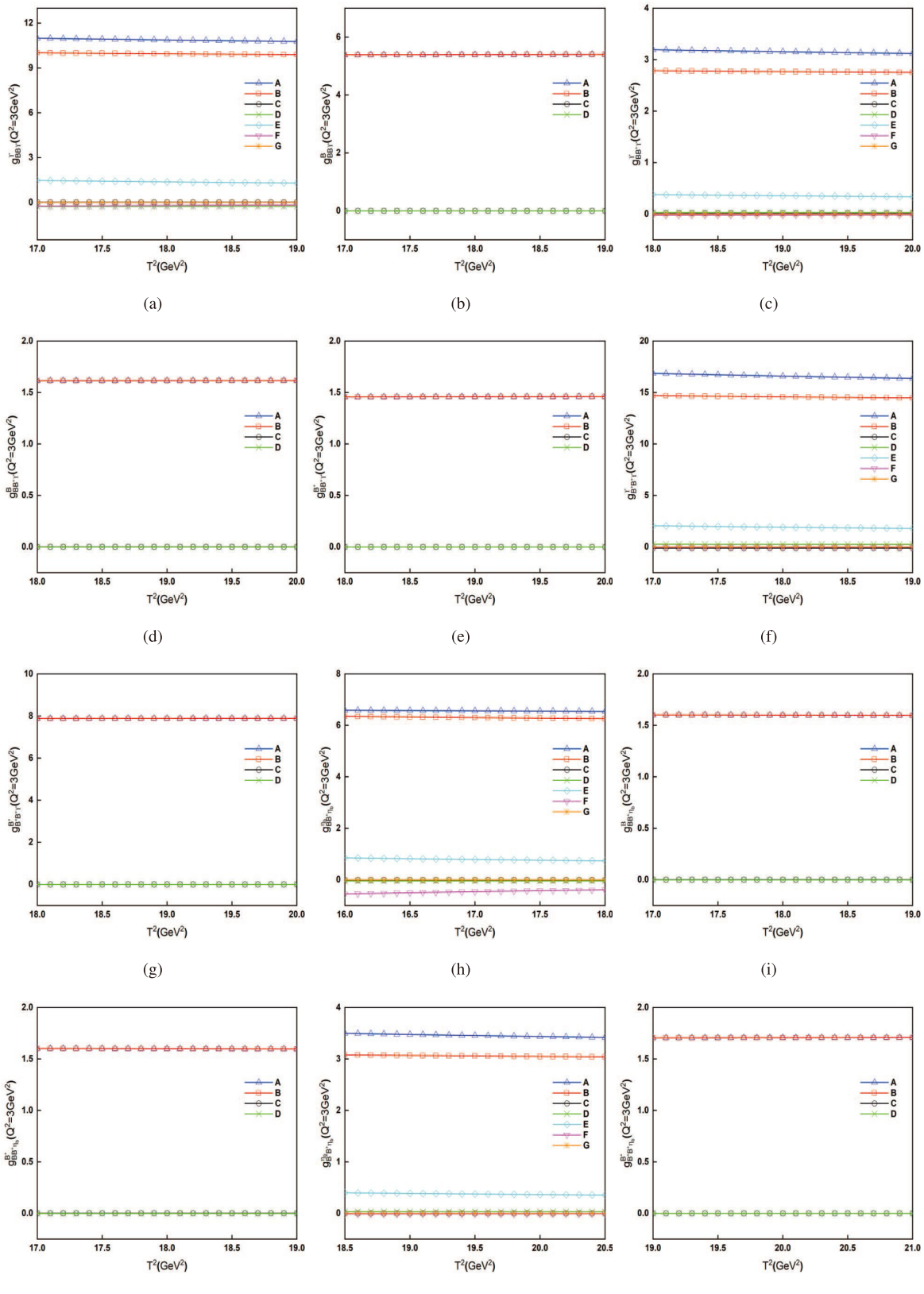

Fig. 6. (color online) Contributions of different vacuum condensate terms with variations of the Borel parameter T^2 for $BB\Upsilon$ (a–b), $BB^*\Upsilon$ (c–e), $B^*B^*\Upsilon$ (f–g), $BB^*\eta_b$ (h–j), and $B^*B^*\eta_b$ (k–l), where A-G denote the total, perturbative, $\langle g_s^2G^2\rangle$,$\langle f^3G^3\rangle$,$\langle\bar{q}q\rangle$,$\langle\bar{q}g_s\sigma Gq\rangle$, and $\langle\bar{q}q\rangle\langle g_s^2G^2\rangle$ contributions.

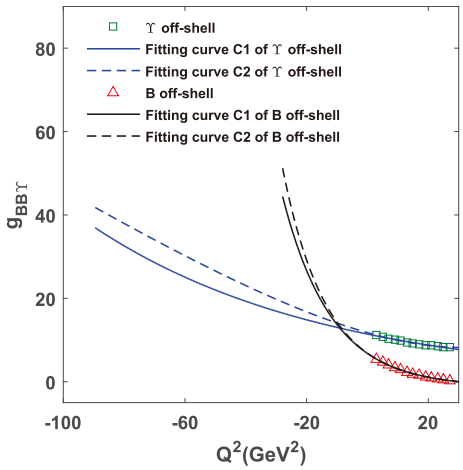

Fig. 7. (color online) Fitting curves of the coupling constants for vertex $BB\Upsilon$ in Υ and B off-shell cases.

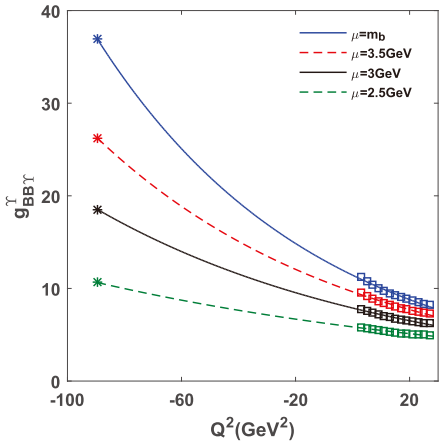

Fig. 8. (color online) Dependence of strong coupling constant $g^{\Upsilon}_{BB\Upsilon}$ on bottom quark mass with different energy-scales.

pendence in Fig. 8 , for which the values are fitted by the $C1$function. From this figure, we can see that the results are indeed strongly dependent on the energy-scale μ. Actually, it is difficult to determine the appropriate energy-scale when calculating the coupling constants with QCDSR or LCSR. In some previous studies, similar calculations were carried out by QCDSR and LCSR with different energy-scales of heavy quarks [45, 47]. In the present study, the strong coupling constants are obtained with the mass of the bottom quark in the energy-scale $\mu = m_b$[50].

Finally, the momentum dependent strong coupling constants can be uniformly fitted into the following analytical function:

$$g(Q^2) = Fe^{-GQ^2} + H, \tag{23}$$

where the values of parameters F, G, and H are as listed in Table 3. The fitting diagrams of strong coupling constants for each vertex are shown in Fig. 9.

Then, $g(Q^2)$ is extrapolated to the time-like regions ($Q^2 < 0$) by Eq. (23), and the on-shell condition is satisfied by setting $Q^2 = -m^2_{\rm on-shell}$. The on-shell values of strong coupling constants for different off-shell cases are obtained and listed in the last column of Table 3.

For each vertex, the on-shell values of coupling constants for different off-shell cases should be equal to each other. For vertex $BB^*\Upsilon$ as an example, the central values for different off-shell cases are $g^{\Upsilon}_{BB^*\Upsilon} = 11.35$ GeV^{-1}, $g^{B}_{BB^*\Upsilon} = 11.36$ GeV^{-1} , and $g^{B^*}_{BB^*\Upsilon} = 12.04$ GeV^{-1}, which are consistent with each other. Thus, it is reasonable to determine the final values of the strong coupling constants by taking their average values. Finally, the results of the strong coupling constants for different strong vertices are determined as

Table 3. Fitting parameters in Eq. (23) and the strong coupling constants for different vertices and off-shell cases.

Vertex	off-shell	F	G	H	$g(Q^2=-m^2_{\rm on-shell})$
$BB\Upsilon$	Υ	11.43	0.013	0	$36.92^{+3.51}_{-3.80}$
	B	7.99	0.062	−1.20	$44.42^{+11.59}_{-4.60}$
$BB^*\Upsilon$	Υ	3.17	0.014	0	$11.35^{+1.01}_{-1.11}$ GeV^{-1}
	B	2.39	0.057	−0.39	$11.36^{+2.31}_{-0.88}$ GeV^{-1}
	B^*	2.17	0.061	−0.33	$12.04^{+3.24}_{-1.29}$ GeV^{-1}
$B^*B^*\Upsilon$	Υ	16.24	0.014	0	$55.10^{+4.67}_{-5.07}$
	B^*	11.63	0.058	−1.84	$58.93^{+5.98}_{-5.55}$
$BB^*\eta_b$	η_b	6.72	0.015	0	$25.52^{+1.84}_{-2.06}$
	B	4.71	0.064	−0.66	$27.31^{+6.35}_{-2.51}$
	B^*	2.39	0.071	−0.28	$17.34^{+6.03}_{-2.34}$
$B^*B^*\eta_b$	η_b	3.48	0.014	0	$11.97^{+1.05}_{-1.41}$ GeV^{-1}
	B^*	2.46	0.060	−0.39	$13.00^{+3.20}_{-1.27}$ GeV^{-1}

$$\begin{aligned} g_{BB\Upsilon} &= 40.67^{+7.55}_{-4.20} \\ g_{BB^*\Upsilon} &= 11.58^{+2.19}_{-1.09}\text{GeV}^{-1} \\ g_{B^*B^*\Upsilon} &= 57.02^{+5.32}_{-5.31} \\ g_{BB^*\eta_b} &= 23.39^{+4.74}_{-2.30} \\ g_{B^*B^*\eta_b} &= 12.49^{+2.12}_{-1.35}\text{GeV}^{-1}. \end{aligned} \tag{24}$$

IV. CONCLUSIONS

In this work, we systematically analyzed the strong vertices $BB\Upsilon$, $BB^*\Upsilon$, $B^*B^*\Upsilon$, $BB^*\eta_b$, and $B^*B^*\eta_b$ using the QCD sum rules, considering all off-shell cases for each vertex. Under this physical sketch, the momentum dependent coupling constants were first obtained in space-like ($Q^2 > 0$) regions and then fitted into appropri-

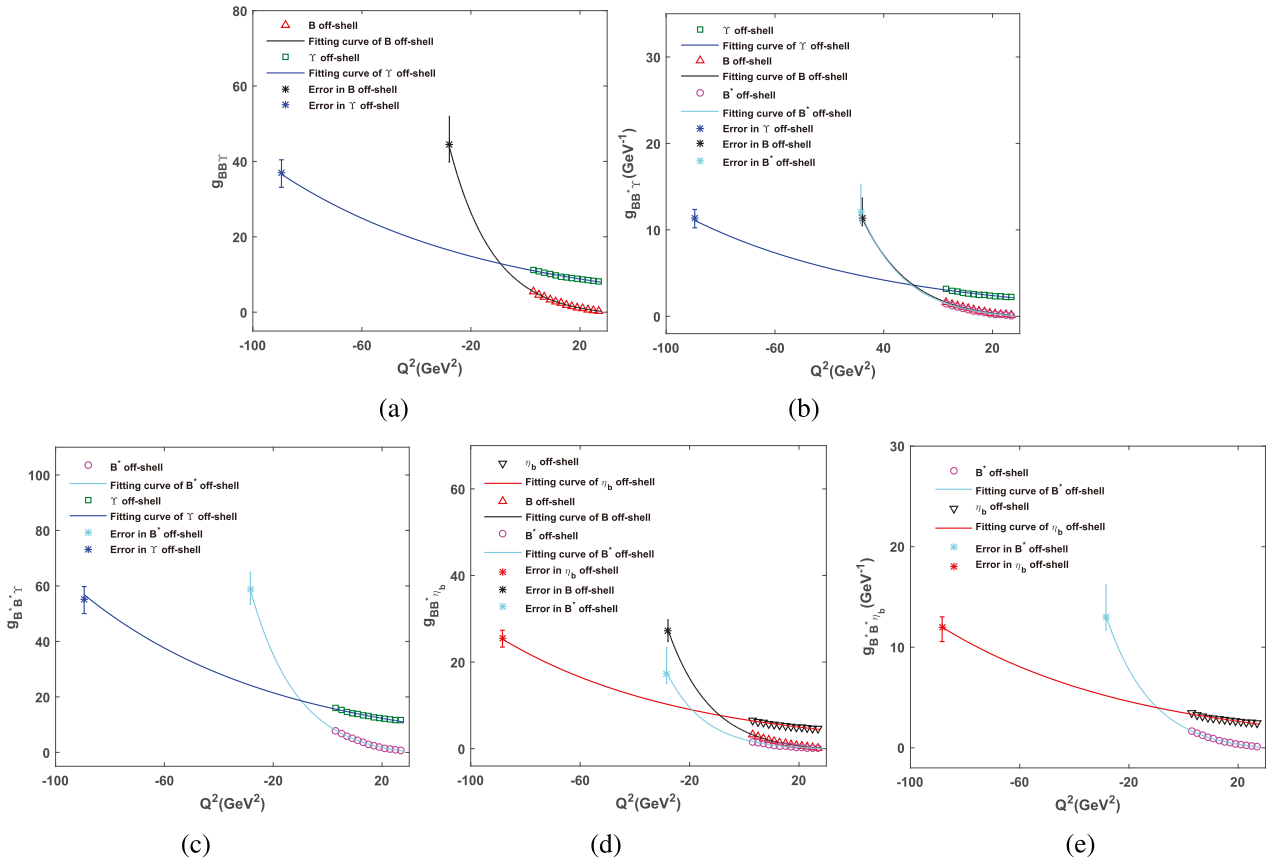

Fig. 9. (color online) Fitting curves of coupling constants for vertices $BB\Upsilon$ (a), $BB^*\Upsilon$(b), $B^*B^*\Upsilon$(c), $BB^*\eta_b$(d), and $B^*B^*\eta_b$(e). In these figures, all possible off-shell cases are considered.

ate analytical functions. By extrapolating these functions to time-like ($Q^2<0$) regions and taking $Q^2=-m^2_{\rm on-shell}$, we obtained the strong on-shell coupling constants. For each vertex, we considered the average value of the strong on-shell coupling constants for all off-shell cases as the final result. These coupling constants are valuable in describing the dynamical behaviors of hadrons. For example, these coupling constants are important input parameters to analyze the final-state interactions in heavy quarkonium decays or to calculate the absorption cross sections for understanding heavy quarkonium absorptions in hadronic matter.

References

[1] T. Matsui and H. Satz, Phys. Lett. B **178**, 416 (1986)
[2] R. Vogt, Phys. Rept. **310**, 197 (1999)
[3] R. Rapp, D. Blaschke, and P. Crochet, Prog. Part. Nucl. Phys. **65**, 209 (2010)
[4] S. G. Matinyan and B. Muller, Phys. Rev. C **58**, 2994 (1998)
[5] K. L. Haglin, Phys. Rev. C **61**, 031902 (2000)
[6] Z. W. Lin and C. M. Ko, Phys. Rev. C **62**, 034903 (2000)
[7] A. Sibirtsev, K. Tsushima, and A. W. Thomas, Phys. Rev. C **63**, 044906 (2001)
[8] Z. W. Lin and C. M. Ko, Phys. Lett. B **503**, 104 (2001)
[9] R. Casalbuoni, A. Deandrea, N. Di Bartolomeo *et al.*, Phys. Rept. **281**, 145 (1997)
[10] C. Meng and K. T. Chao, Phys. Rev. D **78**, 074001 (2008)
[11] F. S. Navarra, M. Nielsen, M. E. Bracco *et al.*, Phys. Lett. B **489**, 319 (2000)
[12] F. S. Navarra, M. Nielsen and M. E. Bracco, Phys. Rev. D **65**, 037502 (2002)
[13] R. Rodrigues da Silva, R. D. Matheus, F. S. Navarra *et al.*, Braz. J. Phys. **34**, 236 (2004)
[14] M. E. Bracco, M. Chiapparini, F. S. Navarra *et al.*, Phys. Lett. B **605**, 326 (2005)
[15] M. E. Bracco, A. Cerqueira, Jr., M. Chiapparini *et al.*, Phys. Lett. B **641**, 286 (2006)
[16] M. E. Bracco, M. Chiapparini, F. S. Navarra *et al.*, Phys. Lett. B **659**, 559 (2008)
[17] M. E. Bracco and M. Nielsen, Phys. Rev. D **82**, 034012 (2010)
[18] B. Osorio Rodrigues, M. E. Bracco, M. Nielsen *et al.*, Nucl. Phys. A **852**, 127 (2011)
[19] K. Azizi and H. Sundu, J. Phys. G **38**, 045005 (2011)
[20] H. Sundu, J. Y. Sungu, S. Sahin *et al.*, Phys. Rev. D **83**, 114009 (2011)
[21] A. Cerqueira, Jr., B. Osorio Rodrigues, and M. E. Bracco, Nucl. Phys. A **874**, 130 (2012)

[22] C. Y. Cui, Y. L. Liu, and M. Q. Huang, Phys. Lett. B **707**, 129 (2012)
[23] C. Y. Cui, Y. L. Liu, and M. Q. Huang, Phys. Lett. B **711**, 317 (2012)
[24] M. E. Bracco, M. Chiapparini, F. S. Navarra *et al.*, Prog. Part. Nucl. Phys. **67**, 1019 (2012)
[25] G. L. Yu, Z. Y. Li, and Z. G. Wang, Eur. Phys. J. C **75**, 243 (2015)
[26] G. L. Yu, Z. G. Wang and Z. Y. Li, Eur. Phys. J. C **79**, 798 (2019)
[27] Z. Y. Li, Z. G. Wang, and G. L. Yu, Mod. Phys. Lett. A **31**, 1650036 (2016)
[28] B. O. Rodrigues, M. E. Bracco, and C. M. Zanetti, Nucl. Phys. A **966**, 208 (2017)
[29] J. Lu, G. L. Yu, and Z. G. Wang, Eur. Phys. J. A **59**, 195 (2023)
[30] P. Colangelo, F. De Fazio, G. Nardulli *et al.*, Phys. Rev. D **52**, 6422 (1995)
[31] T. M. Aliev, N. K. Pak, and M. Savci, Phys. Lett. B **390**, 335 (1997)
[32] P. Colangelo and F. De Fazio, Eur. Phys. J. C **4**, 503 (1998)
[33] Y. B. Dai and S. L. Zhu, Phys. Rev. D **58**, 074009 (1998)
[34] S. L. Zhu and Y. B. Dai, Phys. Rev. D **58**, 094033 (1998)
[35] A. Khodjamirian, R. Ruckl, S. Weinzierl *et al.*, Phys. Lett. B **457**, 245 (1999)
[36] Z. H. Li, T. Huang, J. Z. Sun *et al.*, Phys. Rev. D **65**, 076005 (2002)
[37] H. C. Kim and S. H. Lee, Eur. Phys. J. C **22**, 707 (2002)
[38] Z. G. Wang and S. L. Wan, Phys. Rev. D **73**, 094020 (2006)
[39] Z. G. Wang and S. L. Wan, Phys. Rev. D **74**, 014017 (2006)
[40] Z. G. Wang, Eur. Phys. J. C **52**, 553 (2007)
[41] Z. G. Wang, Nucl. Phys. A **796**, 61 (2007)
[42] Z. G. Wang, Phys. Rev. D **77**, 054024 (2008)
[43] Z. G. Wang and Z. B. Wang, Chin. Phys. Lett. **25**, 444 (2008)
[44] Z. H. Li, W. Liu, and H. Y. Liu, Phys. Lett. B **659**, 598 (2008)
[45] A. Khodjamirian, B. Melić, Y. M. Wang *et al.*, JHEP **03**, 016 (2021)
[46] A. Khodjamirian, C. Klein, T. Mannel and Y. M. Wang, JHEP **09**, 106 (2011)
[47] Z. G. Wang, Phys. Rev. D **89**, 034017 (2014)
[48] L. J. Reinders, H. Rubinstein, and S. Yazaki, Phys. Rept. **127**, 1 (1985)
[49] Y. M. Wang, H. Zou, Z. T. Wei *et al.*, Eur. Phys. J. C **54**, 107 (2008)
[50] R. L. Workman *et al.* (Particle Data Group), PTEP **2022**, 083C01 (2022)
[51] Z. G. Wang, Eur. Phys. J. C **75**, 427 (2015)
[52] D. Bečirević, B. Melić, M. Patra *et al.*, Phys. Rev. D **97**, 015008 (2018)
[53] S. Narison, Phys. Lett. B **693**, 559 (2010), [Erratum: Phys. Lett. B 705, 544 (2011)]
[54] S. Narison, Phys. Lett. B **706**, 412 (2012)
[55] S. Narison, Phys. Lett. B **707**, 259 (2012)